MIYAMOTO, M. & TAKEDA, H. (1984). *Am. Mineral.* **69**, 711–718.
MULHAUSEN, C. & GORDON, R. G. (1981). *Phys. Rev. B*, **23**, 900–923.
ORGEL, L. E. (1961). *An Introduction to Transition Metal Chemistry: Ligand Field Theory*. London: Methuen.
PARKER, S. C. (1982). PhD thesis, Sir Christopher Ingold Laboratories, Univ. College, London.
PAULING, L. (1947). *J. Am. Chem. Soc.* **69**, 542–553.
POST, J. E. & BURNHAM, C. W. (1986). *Am. Mineral.* **71**, 142–150.
PREWITT, C. T., SHANNON, R. D., ROGERS, D. B. & SLEIGHT, A. W. (1969). *Inorg. Chem.* **8**, 1985–1993.
PRICE, G. D. & PARKER, S. C. (1984). *Phys. Chem. Miner.* **10**, 209–216.
RICE, C. E. & ROBINSON, W. R. (1977). *Acta Cryst.* B**33**, 1342–1348.
SASAKI, S., PREWITT, C. T., SATO, Y. & ITO, E. (1982). *J. Geophys. Res.* **87**, 7829–7832.
SHANNON, R. D. (1976). *Acta Cryst.* A**32**, 751–767.
SMYTH, J. R. & HAZEN, R. M. (1973). *Am. Mineral.* **58**, 588–593.
SPEER, J. A. & GIBBS, G. V. (1976). *Am. Mineral.* **61**, 238–247.
TAKAHASHI, I., ONODERA, A. & SHIOZAKI, Y. (1987). *Acta Cryst.* C**43**, 179–182.
TOSSELL, J. A., VAUGHAN, D. J. & JOHNSON, K. H. (1973). *Nature (London) Phys. Sci.* **244**, 42–45.
VINCENT, M. G., YVON, K. & ASHKENAZI, J. (1980). *Acta Cryst.* A**36**, 808–813.
VINCENT, M. G., YVON, K., GRÜTTNER, A. & ASHKENAZI, J. (1980). *Acta Cryst.* A**36**, 803–808.
WALDMANN, M. & GORDON, R. G. (1979). *J. Chem. Phys.* **71**, 1325–1329.
WECHSLER, B. A. & PREWITT, C. T. (1984). *Am. Mineral.* **69**, 176–185.
WECHSLER, B. A. & VON DREELE, R. B. (1989). *Acta Cryst.* B**45**, 542–549.

Acta Cryst. (1992). B**48**, 622–627

Calculated Intensities of Electron Waves Diffracted from Ti–14 wt% Mo Alloy Containing ω-Phase Crystals

BY M. AWAJI, H. HASHIMOTO, E. SUKEDAI AND F. AKAO

Faculty of Engineering, Okayama University of Science, Ridai-cho 1-1, *Okayama* 700, *Japan*

(*Received* 22 *January* 1991; *accepted* 6 *March* 1992)

Abstract

The amplitudes and intensities of electron waves diffracted from a Ti–14 wt% Mo alloy of β-phase containing ω-phase slabs of various thicknesses and at different depths were calculated. The intensities of the forbidden reflections $1/3\ \bar{1}2\bar{1}$, $2/3\ \bar{1}2\bar{1}$ and 121 from the ω_1-phase, which is one of the four variants of the ω-phase, are less than 1.0×10^{-5} even for a thickness of 40 Å. However, when an ω_1-phase of that thickness is included in a crystal of the β-phase at a depth of 80 Å, the intensity of the forbidden reflections increases to about 1.0×10^{-2} at the bottom surface of the ω_1-phase. The amplitudes of the $\bar{1}0\bar{1}$ and $2/3\ \bar{1}2\bar{1}$ waves are proportional to the distance of the ω_1-phase from the top surface and the thickness of that in the β-phase, respectively. When ω_1- and ω_2-phases overlap in the β-phase, extra spots such as $1/3\ \bar{1}0\bar{1}$, $2/3\ \bar{1}0\bar{1}$, 1/3 020 and 2/3 020 are excited at the top surface of the lower variant.

1. Introduction

Since the first observation of the ω-phase formed in aged Ti–Cr alloys (Frost, Parris, Hirsch, Doig & Schwartz, 1954), many studies using electron diffraction patterns and electron microscope images have been reported in other alloy systems (de Fontaine, Paton & Williams, 1971; Sass, 1972). Sukedai & Hashimoto (1989) showed that the projection of the ω_1- and ω_2-phases on the $(10\bar{1})$ plane has an ellipsoidal shape by taking the dark-field images from corresponding diffraction spots. However, the {111} cross section which is perpendicular to the line of apsides of the projected ω-phases within a β-phase has not been studied directly. Even with the cross-sectional observation technique (Marcus & Sheng, 1983), which can be carried out by cutting the specimens in the preferred direction with a diamond saw after molding with epoxy resin and then thinning by ion milling, the structure of the cross section could not be investigated. This is due to the fact that, in the cross-sectional direction, the ω-phases concerned do not produce any characteristic diffraction spots, or any contrast in the electron microscope images because the displacement vectors of atoms **b**, which produce the ω-phases, become parallel to the incident beam. However, calculations of the diffracted wave intensity and of the image contrast in the $[10\bar{1}]$ direction as a function of the thickness and the depth of the ω_1- and ω_2-phases can be used to estimate their thicknesses and positions, and also to understand the mechanism of the appearance of the forbidden reflections.

In this paper, the intensities of diffracted waves for specimens with various types of combination of ω-

0108-7681/92/050622-06$06.00

and β-phase slabs are calculated using the dynamical theory of electron diffraction (Cowley & Moodie, 1957; Goodman & Moodie, 1974) in order to understand the behaviour of diffracted waves due to ω- and β-phases.

2. Model structure and calculation

Calculations were carried out for specimens of Ti–14 wt% Mo alloy which were quenched into water from 1223 K and then aged at 623 K.

The model structure of the ω-phase (de Fontaine & Buck, 1973) is shown in perspective in Fig. 1(*a*), and as a projection on the $(10\bar{1})$ plane in Fig. 1(*b*). A typical electron diffraction pattern from the specimen showing $[10\bar{1}]$ symmetry is shown in Fig. 1(*c*). The arrows in Fig. 1(*a*) indicate the direction of projection of atoms on the $(10\bar{1})$ plane. As can be seen in Figs. 1(*a*) and 1(*b*), the black and shaded dots represent the atoms in the upper and lower planes and atoms in the β-phase alloy (b.c.c.) have the stacking sequence *ABCABC*... along the $[\bar{1}2\bar{1}]$ direction, if the double layers of the $(10\bar{1})$ plane are taken into account. By displacement of atoms *B* and *C* in the directions $\pm[111]$ through a distance $\pm a(3)^{1/2}/12$ (represented by arrows in Fig. 1*b*), the stacking sequence becomes *AIAIAI*... and the ω-phase is produced. It is assumed that the unit cell of the ω-phase has lattice constants three times those of the β-phase, namely $3a = 3b = 3c = 9.855$ Å, $\alpha = \beta = \gamma = 90°$, and also that the unit cell contains only Ti atoms, in conformity with the experimental results of Hickman (1969) that the ω-phase has fewer Mo atoms. Four variants of the ω-phase were produced by displacements to the $\pm[111]$, $\pm[\bar{1}1\bar{1}]$, $\pm[\bar{1}11]$ and $\pm[11\bar{1}]$ directions, and are denoted by ω_1, ω_2, ω_3 and ω_4, respectively.

Calculations were carried out using the following conditions: acceleration voltage = 200 kV; incident-beam direction = $[10\bar{1}]$; number of excited waves = 8192 (including pseudoreflections caused by the large unit cell); no absorption of electron waves in the specimen. The elongation of the diffraction spots in Fig. 1(*c*) may be due to the shape of the ω-phase, and therefore the effect of this elongation was ignored.

3. Results and discussion

Electron diffraction patterns from crystals of the ω-phase with thicknesses of 14 and 140 Å and of $[10\bar{1}]$ symmetry were calculated. 14 Å is about six times the spacing of the $(10\bar{1})$ plane of the β-phase. The results show that the forbidden reflections do not appear at a thickness of 14 Å whereas they do appear at a thickness of 140 Å. This is due to dynamical scattering of electrons in the thicker crystal.

Since the incident beam is in the $[10\bar{1}]$ symmetry direction, the amplitudes of the *hkl* and $\bar{h}\bar{k}\bar{l}$ diffracted waves are the same. The 25 diffracted beams shown in Fig. 2 and the 1/3 444 diffracted beam are discussed in this paper, and for convenience of illustration of the amplitude–thickness curves, the diffracted beams shown in Fig. 2 are classified into six groups *A*, *B*, *C*, *D*, *E* and *F*. Fig. 3 shows the dependence of the amplitudes of the forbidden reflections upon the thickness of the ω_1-phase, whose amplitudes are calculated for unit incident-beam intensity. As can be secn in Fig. 3 (*B*, *C* and *E*), the intensities of the 2/3 $\bar{1}2\bar{1}$, 1/3 $\bar{1}2\bar{1}$ and 121 diffracted beams are of the order of 10^{-5} for thicknesses of 75, 30 and 45 Å, respectively. For the other beams the same order of magnitude of intensity was obtained

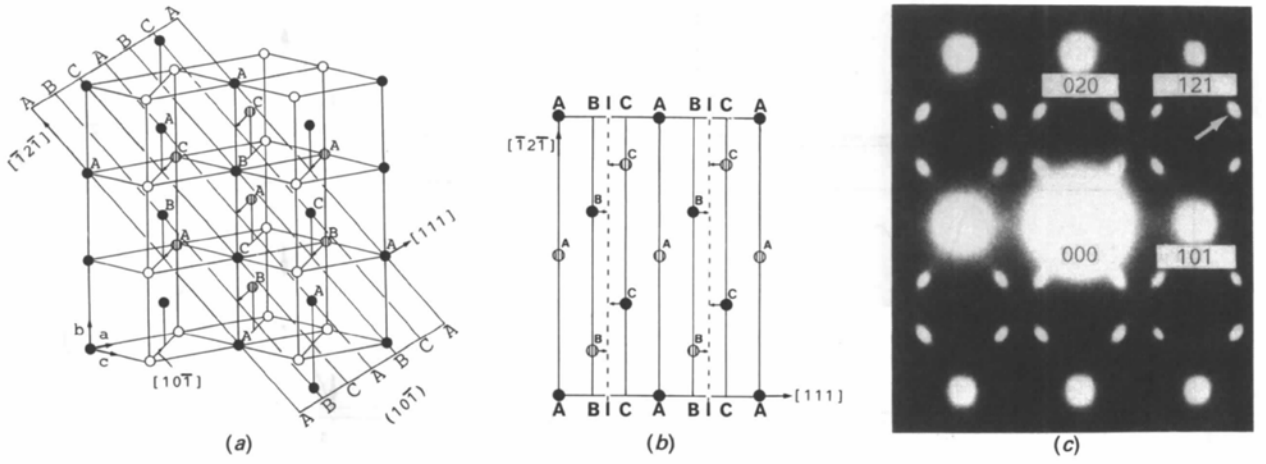

Fig. 1. (*a*) Relation between the β-phase and the $(10\bar{1})$ plane. (*b*) Two-dimensional atom position projected on the $(10\bar{1})$ plane. (*c*) Electron diffraction pattern from an as-quenched Ti–14 wt% Mo alloy.

for thicknesses less than 10 Å. These results suggest that the forbidden reflections appear when the thickness of the ω_1-phase is greater than 75 Å. The amplitudes of these diffracted beams increase gradually and then decrease with increasing thickness of the ω_1-phase. The above discussion for the ω_1-phase can be applied to the ω_2-phase by changing the indices from hkl to $\bar{h}k\bar{l}$. In the case of this incident-

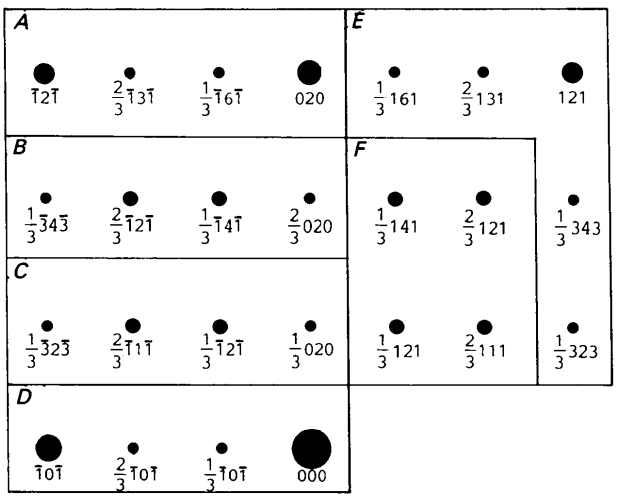

Fig. 2. Classification of electron diffraction spots.

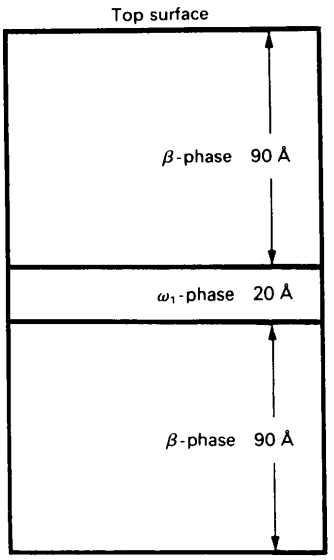

Fig. 4. Cross section of the β-phase containing the ω_1-phase slice.

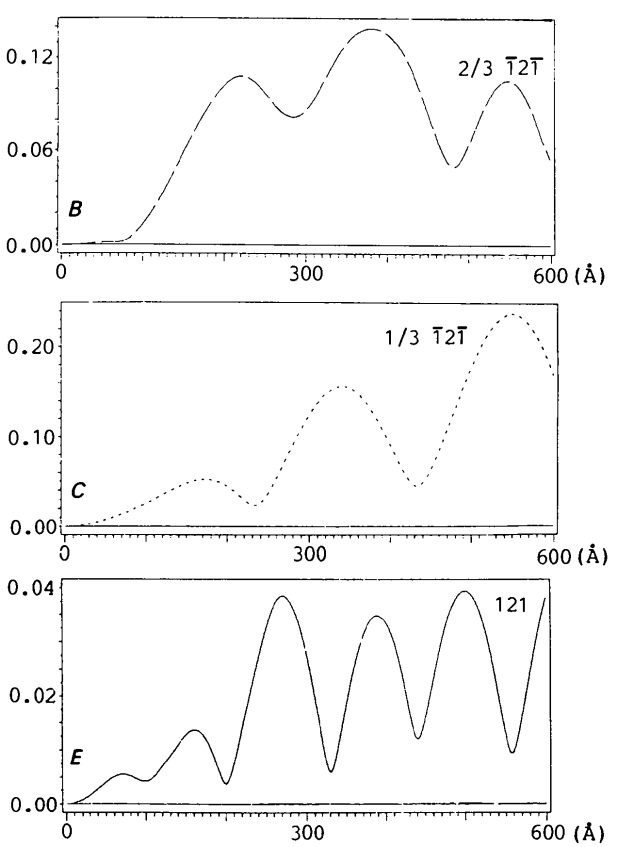

Fig. 3. Calculated amplitudes of the forbidden reflections from the ω_1-phase.

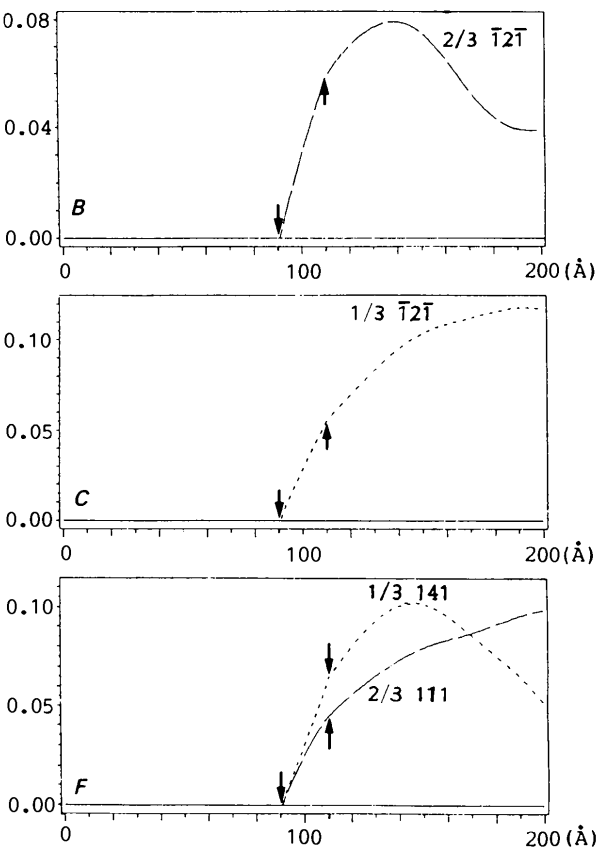

Fig. 5. Calculated amplitudes of the characteristic spots for the model specimen (Fig. 4).

beam direction, the diffraction patterns for the ω_3- and ω_4-phases are the same as for the β-phase, because the displacement of the atoms to form the ω_3- and ω_4-phases cannot be detected in this orientation, and the projected structure becomes almost the same as that of the β-phase.

Fig. 4 shows the cross section of the model structure of a β-phase containing the ω_1-phase slab of thickness 20 Å. Fig. 5 shows the variation of amplitudes against the depth measured from the top surface of the model specimen. The characteristic spots 2/3 $\bar{1}2\bar{1}$, 1/3 $\bar{1}2\bar{1}$, 2/3 111 and 1/3 141 appear at 90 Å in depth and their amplitudes increase rapidly, especially the amplitudes of the 2/3 $\bar{1}2\bar{1}$ and 1/3 $\bar{1}2\bar{1}$ diffracted waves, which show a noticeable increase in comparison with the behavior shown in Fig. 3. This seems to be due to the effect of scattering in the top β-phase. However, the increments of the amplitudes of the characteristic reflections become small at a depth larger than 110 Å. These results suggest the following two facts. Firstly, the amplitudes of these characteristic spots are excited only in the ω_1-phase and even after passing through the ω_1-phase they still increase in the bottom β-phase. Secondly, even when the ω_1-phase is only a few ångstroms in thickness it may produce noticeable intensity in these four diffracted beams. These characteristics do not change even when the ω_1-phase slab of thickness 20 Å is located at depths of $\frac{1}{4}$, $\frac{1}{2}$ and $\frac{3}{4}$ of the total thickness of the β-phase of Fig. 4, with the exception that the amplitude of the 2/3 111 beam decreases after entering the bottom β-phase for the case when the ω_1-phase is located at a depth of $\frac{3}{4}$ of the total thickness.

Fig. 6 shows cases where the ω_1-phase slab in the β-phase is located between the two arrows. By comparing these three figures, it is seen that the amplitude of the $\bar{1}0\bar{1}$ diffracted beam at a depth of 200 Å is proportional to the depth of the ω_1-phase slab with a proportionality constant of 9×10^{-3}.

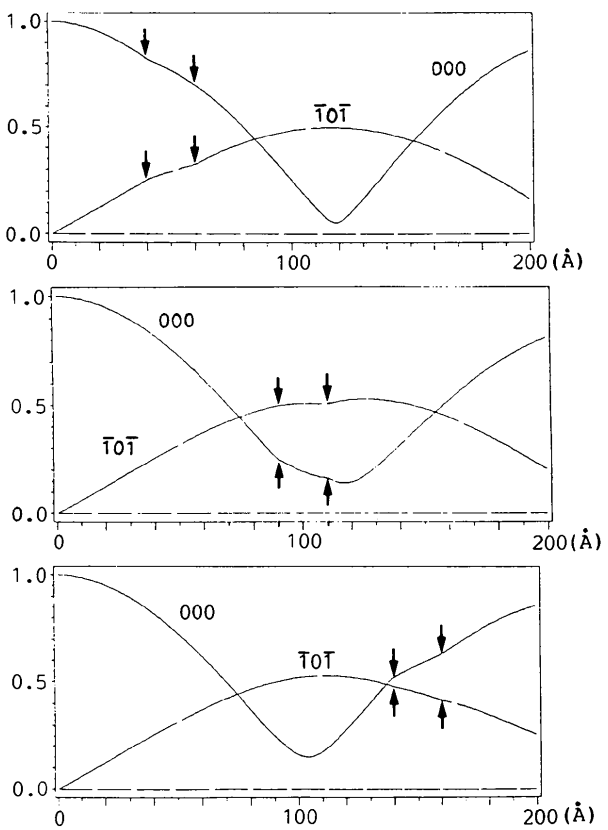

Fig. 6. Behavior of the amplitude of the $\bar{1}0\bar{1}$ wave.

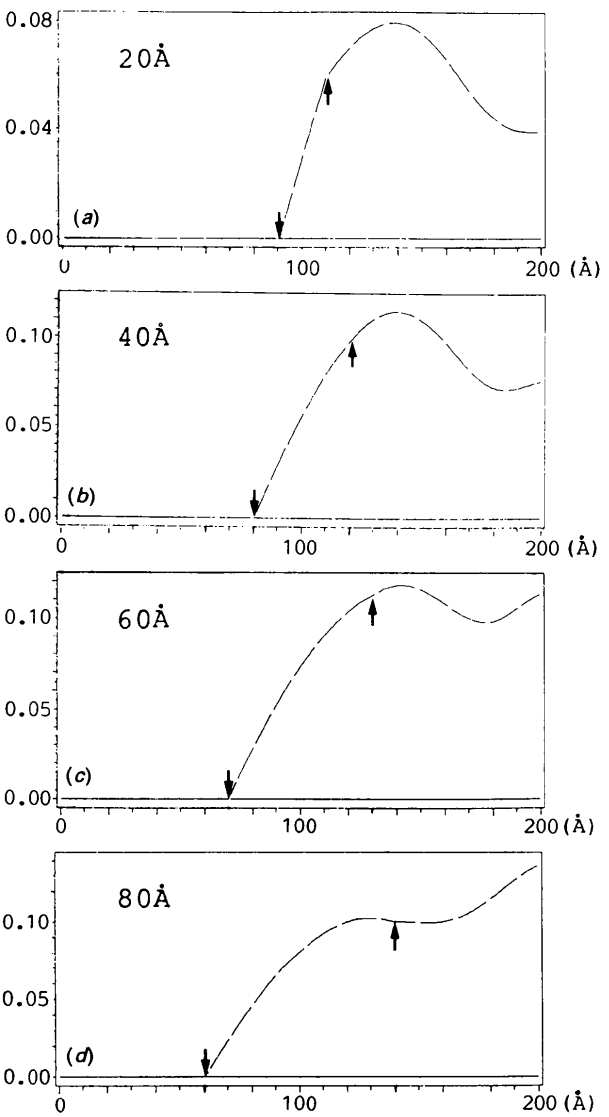

Fig. 7. Behavior of the amplitude of the 2/3 $\bar{1}2\bar{1}$ wave for ω_1-phase thicknesses of (*a*) 20, (*b*) 40, (*c*) 60 and (*d*) 80 Å.

Fig. 7 shows the behavior of the amplitude of the $2/3\ \bar{1}2\bar{1}$ beam. The ω_1-phase with thicknesses of 20, 40, 60 and 80 Å in the β-phase is located between the two arrows. The amplitude of the beam at a depth of 200 Å (*i.e.* at the bottom surface of the model specimen) is proportional to the thickness of the ω_1-phase with an average proportionality constant 1.6×10^{-2}. In spite of the fact that the amplitude at a depth of 140 Å shown in (*d*) is smaller than those in (*b*) and (*c*), the amplitude at a depth of 200 Å in (*d*) is larger. It therefore seems to be possible to derive the position and the thickness of the ω_1- and ω_2-phase slabs in the β-matrix by measuring the intensities of these diffracted beams.

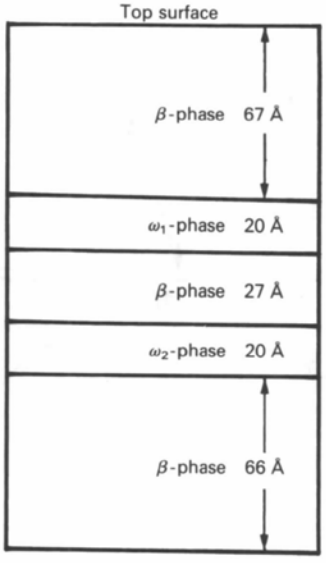

Fig. 8. Cross section of the β-phase containing the ω_1- and ω_2-phase slabs.

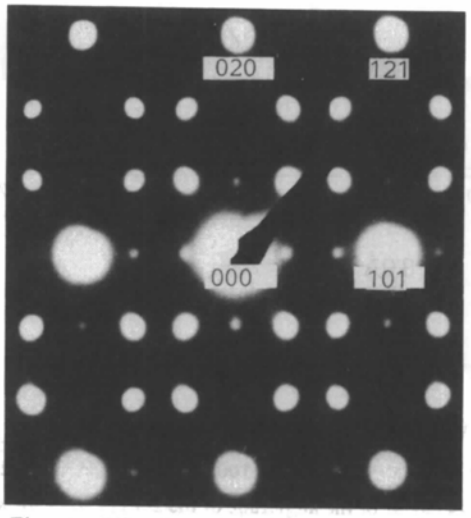

Fig. 9. Electron diffraction pattern from a well aged specimen.

The $1/3(444)$ plane of the ω_1-phase is the *I* plane of high atomic density as shown in Fig. 1(*b*). The corresponding observed diffracted beam is indicated by an arrow in Fig. 1(*c*). When the ω_1-phase of thickness 30 Å is located in the β-phase with a thickness of 200 Å, the calculated intensity of the $1/3\ 444$ diffracted beam increases rapidly in the ω_1-phase but decreases gradually on entering the bottom β-phase. This behavior was independent of the position of the ω_1-phase. Also the intensity of the beam at a depth of 200 Å becomes similar to that of the other diffracted beams, in agreement with observations.

In some parts of a specimen, it was observed that there were some overlapping regions of the ω_1- and

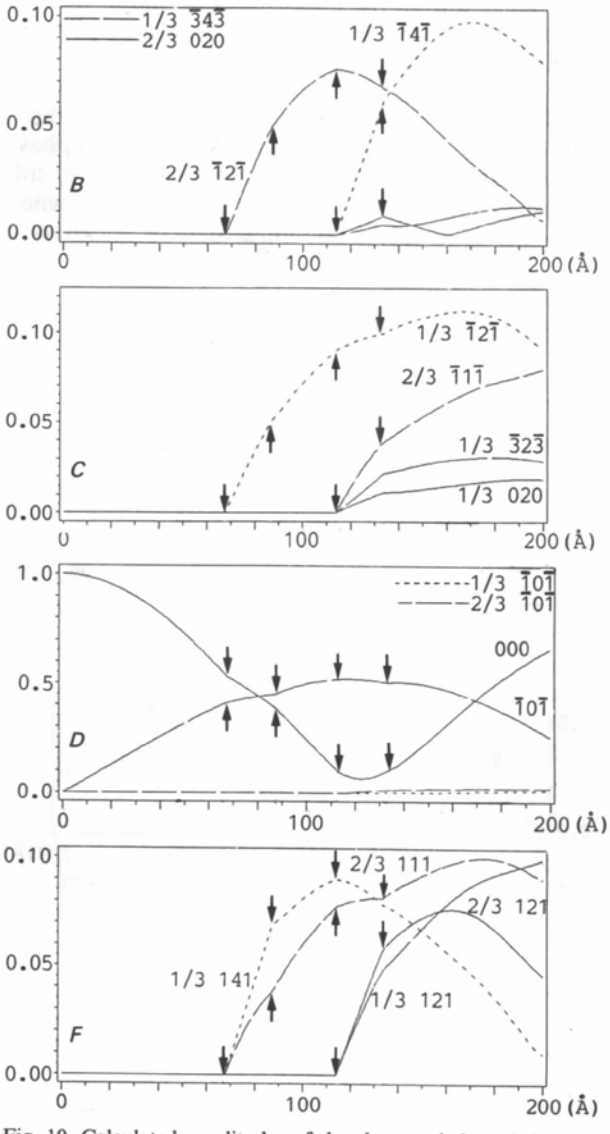

Fig. 10. Calculated amplitudes of the characteristic and the extra spots for the model specimen (Fig. 8).

ω_2-phases in the β-phase (Sukedai, Hashimoto & Tomita, 1991) which can be expressed by the model shown in Fig. 8. In this model the β-phase containing only ω_3- and ω_4-phases gives the diffraction pattern for the β-phase only. Thus, if the ω_2-phase in their model is replaced by the ω_1-, ω_3- or ω_4-phase, the calculated diffraction patterns are similar to those calculated for the model shown in Fig. 4. The extra spots were observed for a specimen aged for 28 h (Fig. 9) in which the well developed ω-phases are superimposed in the manner of the model. Fig. 10 shows the amplitudes of the characteristic and the extra diffraction spots for the model specimen and the arrows indicate the phase boundaries shown in Fig. 8. The intensities of the extra spots appear from the top surface of the ω_2-phase and the intensity of the $1/3\ \bar{1}0\bar{1}$ beam is weaker than that of the $2/3\ \bar{1}0\bar{1}$ beam. This tendency does not change with the position of the ω_1–β–ω_2 sandwich at depths of $\frac{1}{3}$, $\frac{1}{2}$ and $\frac{2}{3}$ of the total thickness. This does not agree with the experimental result shown in Fig. 9 and it seems to be due to the difference in the number and modes of the sandwich realized in the specimen. There are also some intensity asymmetries in hkl and $\bar{h}k\bar{l}$ in Fig. 10. This may be due to differences in the superposition sequence of ω_1- and ω_2-phases.

The authors thanks are due to Mrs Y. Li for her help in taking the photograph (Fig. 9) and to Dr M. J. Whelan, FRS, for reading the manuscript.

References

COWLEY, J. M. & MOODIE, A. F. (1957). *Acta Cryst.* **10**, 609–619.

FONTAINE, D. DE & BUCK, O. (1973). *Philos. Mag.* **27**, 967–983.

FONTAINE, D. DE, PATON, N. E. & WILLIAMS, J. C. (1971). *Acta Metall.* **19**, 1153–1162.

FROST, P. D., PARRIS, W. M., HIRSCH, L. L., DOIG, J. R. & SCHWARTZ, C. M. (1954). *Trans. Am. Soc. Met.* **46**, 231–251.

GOODMAN, P. & MOODIE, A. F. (1974). *Acta Cryst.* A**30**, 280–290.

HICKMAN, B. S. (1969). *Trans. Metall. Soc. AIME*, **245**, 1329–1336.

MARCUS, R. B. & SHENG, T. T. (1983). *Transmission Electron Microscopy of Silicon VLSI Circuits and Structures*, pp. 19–26. New York: John Wiley.

SASS, S. L. (1972). *J. Less Common Met.* **28**, 157–173.

SUKEDAI, E. & HASHIMOTO, H. (1989). *EMAG-MICRO89 London*, No. 98, pp. 371–374.

SUKEDAI, E., HASHIMOTO, H. & TOMITA, M. (1991). *Philos. Mag. A*, **64**, 1201–1208.

Acta Cryst. (1992). B**48**, 627–632

Nitro–Nitrito Linkage Photoisomerization in Crystals of Pentaamminenitrocobalt(III) Dichloride

BY MARI KUBOTA AND SHIGERU OHBA*

Department of Chemistry, Faculty of Science and Technology, Keio University, Hiyoshi 3, *Kohoku-ku, Yokohama* 223, *Japan*

(*Received* 20 *January* 1992; *accepted* 8 *April* 1992)

Abstract

Photoisomerization in $[Co(NH_3)_5NO_2]Cl_2$ has been investigated by single-crystal X-ray diffraction: M_r = 261.0, monoclinic, $C2/c$, $Z = 4$, $D_x = 1.83$ Mg m^{-3}, λ(Mo $K\alpha$) = 0.71073 Å, $\mu = 2.35$ mm^{-1}, $F(000)$ = 536, $T = 116$ K. Before illumination with an Xe lamp, (I*a*), $a = 10.176$ (2), $b = 8.692$ (1), $c = 10.746$ (2) Å, $\beta = 95.45$ (2)°, $V = 946.2$ (3) Å^3, $R = 0.028$ for 1263 observed unique reflections. After illumination with an Xe lamp for 40 min, (I*b*), $R = 0.042$ for 1216 reflections. After illumination for 150 min, (I*c*), R = 0.062 for 730 reflections. Variation of the lattice constants was less than 0.6%. Nitrito coordination, induced by photochemical reaction, was detected on electron density maps and the populations were refined to (I*b*) 8.9 (5)% and (I*c*) 14.5 (8)%. Thermodynamical linkage isomerization in $[Co(NH_3)_5ONO]Cl_2$, (II), was reinvestigated based on the X-ray intensity data measured by Grenthe & Nordin [*Inorg. Chem.* (1979), **18**(7), 1869–1874]. Linkage isomerization occurs in the original plane of NO_2^- in (I). However, the nitro plane is inclined during isomerization of (II) because of steric hindrance to rotation in the original plane.

Introduction

The nitrite ion is ambidentate and coordinates to metal atoms *via* an oxygen, nitrogen or two oxygen atoms (Finney, Hitchman, Raston, Rowbottom &

* To whom correspondence should be addressed.

0108-7681/92/050627-06$06.00